Nanoscale

PAPER

View Article Online
View Journal | View Issue

Cite this: *Nanoscale*, 2015, **7**, 10101

The defect level and ideal thermal conductivity of graphene uncovered by residual thermal reffusivity at the 0 K limit†

Yangsu Xie,[a] Zaoli Xu,[a] Shen Xu,[a] Zhe Cheng,[a] Nastaran Hashemi,[a] Cheng Deng[a] and Xinwei Wang*[a,b]

Received 29th March 2015,
Accepted 29th April 2015

DOI: 10.1039/c5nr02012c

www.rsc.org/nanoscale

Due to its intriguing thermal and electrical properties, graphene has been widely studied for potential applications in sensor and energy devices. However, the reported value for its thermal conductivity spans from dozens to thousands of W m^{-1} K^{-1} due to different levels of alternations and defects in graphene samples. In this work, the thermal diffusivity of suspended four-layered graphene foam (GF) is characterized from room temperature (RT) down to 17 K. For the first time, we identify the defect level in graphene by evaluating the inverse of thermal diffusivity (termed "thermal reffusivity": Θ) at the 0 K limit. By using the Debye model of $\Theta = \Theta_0 + C \times e^{-\theta/2T}$ and fitting the Θ–T curve to the point of T = 0 K, we identify the defect level (Θ_0) and determine the Debye temperature of graphene. Θ_0 is found to be 1878 s m^{-2} for the studied GF and 43–112 s m^{-2} for three highly crystalline graphite materials. This uncovers a 16–43-fold higher defect level in GF than that in pyrolytic graphite. In GF, the phonon mean free path solely induced by defects and boundary scattering is determined as 166 nm. The Debye temperature of graphene is determined to be 1813 K, which is very close to the average theoretical Debye temperature (1911 K) of the three acoustic phonon modes in graphene. By subtracting the defect effect, we report the ideal thermal diffusivity and conductivity (κ_{ideal}) of graphene presented in the 3D foam structure in the range of 33–299 K. Detailed physics based on chemical composition and structure analysis are given to explain the κ_{ideal}–T profile by comparing with those reported for suspended graphene.

1. Introduction

Graphene, a form of carbon with a monolayer honeycomb lattice, has been the focus of extensive investigations since its discovery in 2004. Due to a number of intriguing properties, such as extremely high electrical[1] and thermal conductivity,[2] mechanical strength to weight ratios,[3] and large specific surface area,[4] graphene has become an attractive candidate for promising applications in various areas. Potential graphene applications include lightweight and flexible touch screens,[5] electric circuits,[6] solar cells,[7] next generation batteries,[8] low cost water desalination,[9] drug delivery,[10] *etc*. Understanding the fundamental physics and the underlying mechanism controlling those amazing properties can pave the way for its wide applications.

Among its numerous outstanding properties, the highest thermal conductivity (κ) is of significant importance for graphene's applications. Different approaches have been developed to characterize the thermal conductivity of graphene. The first experimental measurement was conducted at the University of California Riverside[2] using a "noncontact technique based on micro-Raman spectroscopy". In their experiment, an extremely high thermal conductivity of single-layered graphene was found in a range of $(4.84 \pm 0.44) \times 10^3$ to $(5.30 \pm 0.48) \times 10^3$ W m^{-1} K^{-1} at RT. This value exceeds the measured thermal conductivity of other carbon materials, such as CNTs and diamond. As for isotopically pure ^{12}C graphene, the in-plane thermal conductivity was determined to be higher than 4000 W m^{-1} K^{-1} at 320 K by Chen *et al.* using the optothermal Raman technique.[11] Despite the reported high conductivity, other smaller values were also obtained. Lee *et al.* performed measurements for suspended pristine SLG using Raman scattering spectroscopy. The resulting thermal conductivity is ~1800 W m^{-1} K^{-1} near 325 K to ~710 W m^{-1} K^{-1} near 500 K.[12] Faugeras *et al.* obtained value ≈630 W m^{-1} K^{-1} at a temperature of about 600 K by employing micro-Raman scattering experiments for the suspended large graphene membrane.[13]

[a]*Department of Mechanical Engineering, Iowa State University, Ames, IA 50011, USA. E-mail: xwang3@iastate.edu; Tel: +1 515 2948023*
[b]*School of Urban Development and Environmental Engineering, Shanghai Second Polytechnic University, Shanghai 201209, P. R. China*
†Electronic supplementary information (ESI) available. See DOI: 10.1039/c5nr02012c

Their graphene membranes were obtained by depositing large graphene crystals onto a silicon wafer. Many impurities resulted from the PMMA copper film and acetone may exist due to the sample fabrication process.

A large discrepancy exists between these experimental results. So far the value of the measured κ of graphene ranges from dozens to thousands of W m^{-1} K^{-1}. The lower bound can be further lowered for more defective samples.[14] This discrepancy can be induced by many factors: mainly the sample defects, different isotope compositions, substrate effects, different temperatures and uncertainties in the measurements. Some factors can be controlled and compared. Coupling and phonon scattering at the substrate can be averted by suspending graphene samples.[2,15,16] The isotope purified and structured uniform monolayer graphene has also been measured and studied.[11] However, the defect level in the samples is extremely difficult to measure. Defects including charged impurities,[17] functionalized groups,[18] Stone–Wales defects, vacancy defects, stains, *etc*. are complex and random, and hard to interpret in detail. Obtaining the ideal thermal conductivity of different graphene samples experimentally remains a challenge. Given the difficulty of the experiment, theoretical modeling and simulation play an important role in investigating the ideal thermal properties of graphene. Nika *et al.* calculated the thermal conductivity of graphene using the valence-force field method. The obtained thermal conductivity of single-layered graphene ranges from 2000 to 5000 W m^{-1} K^{-1} depending on the flake size, edge roughness and defect concentration.[19] Zhang *et al.* characterized the thermo-physical properties of 2D graphene nanoribbons using the transient molecular dynamics technique. Quantum correction was applied in temperature calculations, and a thermal conductivity of 149 W m^{-1} K^{-1} at 692.3 K and 317 W m^{-1} K^{-1} at 300.6 K was obtained for the 1.99 nm wide GNR with infinite length.[20] Other results using MD simulations,[21] Boltzmann transport equation[22] and Ballistic theory[23] predicted the ideal thermal conductivity. It was found that without defect scattering, κ spans a range of 2400–10 000 W m^{-1} K^{-1} depending on different graphene flake sizes.

Compared to 2D graphene sheets, three-dimensional graphene macro-scale foam (GF) with controllable microscopic structure is mechanically robust and thus greatly simplifies the experimental measurement. As one of the most promising forms of graphene for practical application, GF has attracted wide attention.[24–26] Its continuously and covalently bonded structure makes it possible to overcome the interface thermal resistance for application as thermal interface materials.[27] Pettes *et al.* investigated the effects of processing conditions on the thermal conductivity of GF (κ_{GF}).[27] They obtained κ_{GF} directly by measuring the electrical resistance during electrical heating. It was found that κ_{GF} follows a quadratic correlation with temperature at low temperature and has a peak of 250–650 W m^{-1} K^{-1} at about 150 K. This work revealed the different dominant phonon scattering mechanisms from low temperature to near RT for GF. The low effective κ_{GF} was attributed to the very low volume fraction and high porosity. Lin *et al.* studied the thermal diffusivity of GF samples at RT using the transient electro-thermal (TET) technique. The radiation effect was excluded rigorously by measuring GF samples at different lengths. The intrinsic κ of the two-layered graphene inside GF was originally determined without measuring the porosity of the GF sample, which highly improved the accuracy of thermal characterization of graphene from GF experiments.[15]

In this work, we experimentally investigate the thermal diffusivity of GF samples varying with temperature ranging from RT to 17.0 K. Using the Schuetz's model, the intrinsic thermal diffusivity of graphene was determined accurately. A novel method is presented to subtract the defect scattering effects and obtain the ideal thermal conductivity of graphene. Using the concept of thermal reffusivity, we identify the defect effect and the Debye temperature of graphene. Finally, the ideal thermal conductivity of graphene in the temperature range of 33 K to RT is presented. The results are discussed and further interpreted by comparing with other studies.

2. Sample characterization and methods for thermal characterization

The graphene foam (purchased from Advanced Chemical Supplier Material Company) was synthesized by the chemical vapor deposition (CVD) method. Fig. 1(a) and (b) show the images of GF samples under a scanning electron microscope (SEM) from low to high magnification, where 3D porous foam-like structure of GF can be clearly seen. Fig. 1(c) presents the Raman spectrum of the GF sample. The ratio of the integrated intensity of G band to that of 2D band (I_G/I_{2D}) is 0.63, indicating that there are about 4 layers of graphene in our GF sample.[28] The crystal structure was examined by X-ray diffraction (XRD) analysis presented in Fig. 1(c) and (d). The fitting results in an interlayer spacing of 3.35 Å, which is very close to the reported value of 3.4 nm for bilayered and three-layered graphene.[29] The XPS result shows that the GF is mainly composed of carbon (89%), oxygen (8.43%), nitrogen (0.43%), and silicon (2.14%). Fig. 1(e) shows the C 1s spectrum of GF. The N 1s is presented in Fig. 1(f), indicating the presence of a small amount of the NH–C═O functional group on the surface of GF samples.[30] Details of the structure characterization can be found in the ESI.†

The thermal diffusivity of GF samples at different temperatures was measured to study how the thermal diffusivity varies with decreasing temperature. A Janis closed cycle refrigerator (CCR) system is employed to provide a stable and reliable environmental temperature from 295 K to 10 K. The transient electro-thermal (TET) technique developed by our laboratory is used in the experiment. The TET technique has been proven to be an accurate and reliable approach to measuring the thermal diffusivity of various solid materials, including conductive, semi-conductive or nonconductive materials. The thermal diffusivity of different materials, such as micro-scale

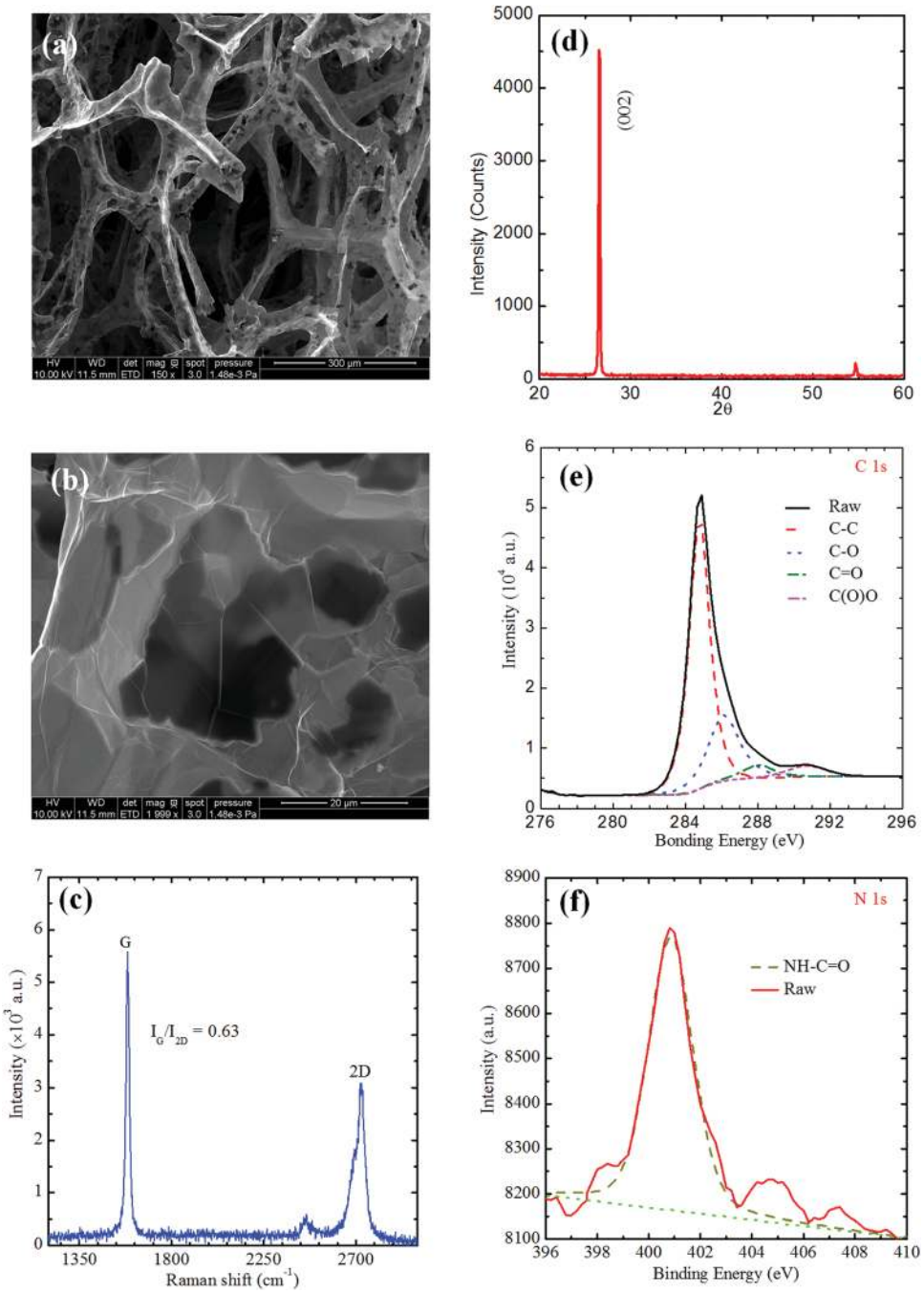

Fig. 1 SEM, Raman and XRD spectra images of the GF sample studied in this work. (a) and (b): SEM images of GF cellular structure and wall structure respectively. (c) Raman spectrum of the GF sample. Raman conditions: CW laser at 532 nm wavelength, 100× lens, and 10 s integration time. I_G/I_{2D} is the ratio of the integrated intensity of the G band to that of the 2D band. The value of I_G/I_{2D} indicates that the GF is composed of about 4-layered graphene. (d) XRD spectrum of the GF sample. The fitting result reveals a pronounced peak at 26.6°, yielding an interlayer spacing of 3.35 Å. (e) and (f) X-ray photoelectron spectra of GF. (e) The C 1s spectrum, indicating different bonds for carbon atoms in the sample. The C–C bond takes the majority, while some other bonds like C–O, C=C, and C(O)O also exist. (f) The N 1s spectrum, suggesting the presence of the NH–C=O functional group at the surface of the samples.

polyester fibers,[31] micro/nanoscale thin films composed of anatase TiO_2 nanofibers,[32] single-walled carbon nanotubes,[33] DNA fibers,[34] silkworm silks,[35] *etc.*, were measured successfully using the TET technique. The obtained results have a high accuracy with less than 5% difference compared to the values in references. Fig. 1(a) shows the schematic of the TET experiment. The detailed experimental process and principles for TET can be found in the ESI.† The measured thermal

diffusivity from TET is a combination of the real thermal diffusivity and the radiation effect:

$$\alpha_{\text{measure}} = \alpha + \frac{1}{\rho c_p}\frac{8\varepsilon_r \sigma T_0^{\,3}}{D}\frac{L^2}{\pi^2}, \quad (1)$$

where α_{measure} is the measured thermal diffusivity, and α is the real thermal diffusivity of GF. ε_r is the effective heat emissivity of GF, and $\sigma = 5.67 \times 10^{-8}$ W m^{-2} K^{-4} is the Stefan–Boltzmann constant. D and L are the thickness and length of the sample, respectively. T_0 is the environmental temperature and ρc_p is the specific heat of graphene foam per unit volume.

TET measurements were conducted at every 25 K of environmental temperature from 295 K to 100 K. Denser data points are collected at low temperatures (<100 K) to have a clearer view of low temperature effects. After that, the sample is taken out and cut shorter for the next experiment. Experiments are repeated with the same sample with three different lengths. The measured samples are detailed in Table 1. The voltage evolution (V_{exp}) was recorded using an oscilloscope (Tektronix DPO 3052 Digital Phosphor Oscilloscope). As a zero-gap semiconductor, graphene's resistance is inversely proportional to its increasing temperature, which should be linearly reflected in the decreasing voltage in our TET measurement. The inset in Fig. 2(b) shows the resistance against temperature profile for sample 1 from 295 K to 10 K,

Table 1 Details of GF samples characterized in this work

Sample	Sample_1	Sample_2	Sample_3
Length (mm)	5.14	3.74	1.01
Width (mm)	1.37	1.38	1.37

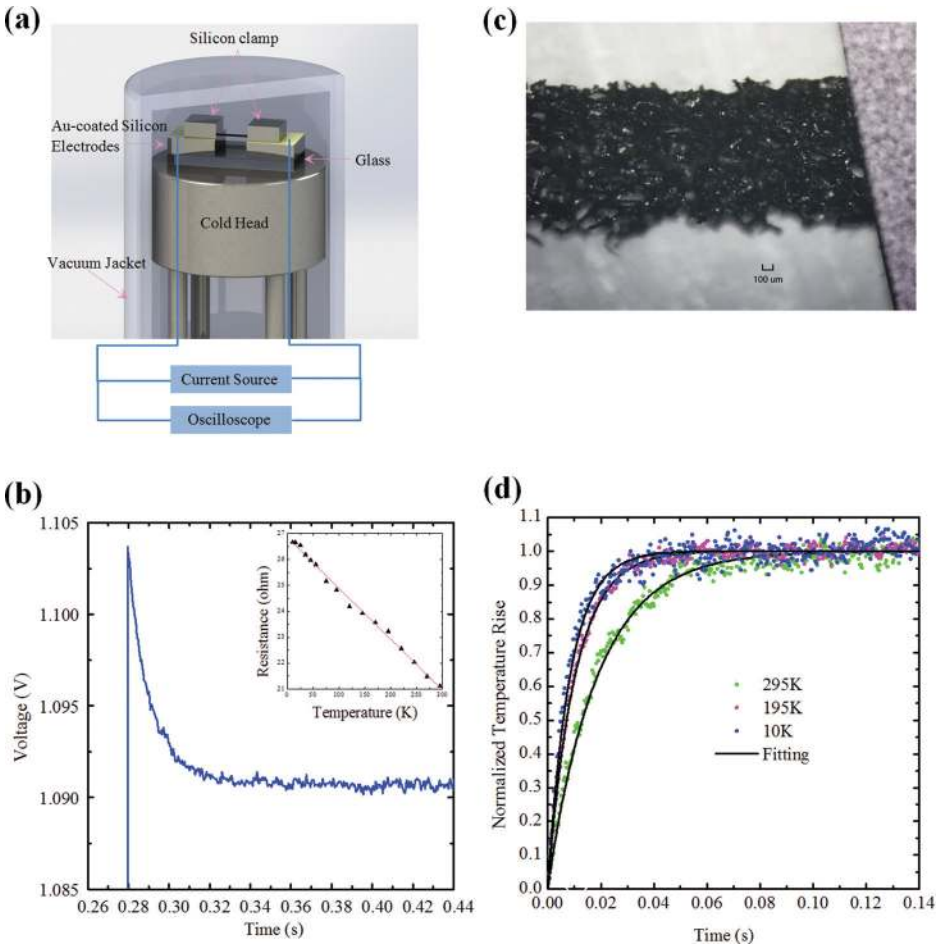

Fig. 2 (a) Schematic of the experimental setup and data collection for the TET technique. The GF sample is suspended between two gold-coated silicon electrodes and compressed tightly by two smooth silicon wafers. The whole sample base is mounted on the cold head of the CCR system. A current source supplies the step current and an oscilloscope records the voltage evolution for the GF sample. (b) The raw voltage against time data collected by the oscilloscope for sample 1 at the environmental temperature of 195 K. The inset demonstrates the linear relationship between resistance and temperature for sample 1 from 295 K to 10 K. (c) Microscopy image of the GF sample (sample 1) suspended between two gold-coated silicon electrodes. (d) Theoretical fitting of the normalized temperature rise for sample 1 at different environmental temperatures: 295 K, 195 K, and 10 K. Dots represent the experimental data and solid lines show the fitting result. These experiments are conducted in a vacuum lower than 0.5 mTorr. The time for reaching the steady state in TET measurements becomes shorter and shorter as T_0 decreases from 295 K to 10 K, demonstrating that the measured thermal diffusivity increases with decreasing temperature.

which confirms the linear R–T relationship. A linear fitting can be used to describe the R–T relationship: $R = 26.85–0.0196 \times T$. Fig. 2(b) shows one of the voltage evolutions (sample 1 at 195 K). The voltage before electrical heating is 1.104 V. Upon the step current, the voltage begins to decrease and finally reaches a steady voltage at about 1.091 V, resulting in the voltage change of 1.18%. Given that the step current for this measurement is 47.2 mA, the resistance can be calculated as 23.39 Ω and 23.11 Ω before and after the heating respectively. Based on the linear R–T relationship of sample 1, the temperature increase is determined as 14.29 K. The recorded experimental V–t data are theoretically fitted using different trial values of the thermal diffusivity subsequently. Using eqn (2) in the ESI† and MATLAB programming, the experimental data are fitted by comparing with the theoretical curve with different trial values of measured thermal diffusivity ($\alpha_{measure}$). Applying the least squares fitting technique, the value giving the best fit of V_{exp} is taken as $\alpha_{measure}$. The $\alpha_{measure}$ represents the thermal diffusivity during the joule heating process. The corresponding real temperature can be approximated by the average of the environmental temperature (T_0) and the stable temperature of the sample (T_1). Here, the real temperature (T) is taken as 195 + 14.29/2 ≈ 202 K. To determine the uncertainty of the fittings, different trial values are also used for the fitting. It is found that when the trial values are changed by ±10%, the fitting curve obviously deviates from the experimental data. Thus the fitting uncertainty was estimated as 10%, but the real error should be much smaller since we measured each value of thermal diffusivity 30 times and took the average value as the final thermal diffusivity. In this example, $\alpha_{measure}$ is determined as 2.38×10^{-4} m^2 s^{-1} at the real temperature of 202 K. The normalized temperature rise can be obtained using $T^* = [V(t) - V_0]/[V(t \to \infty) - V_0]$. Fig. 2(d) shows the normalized temperature rise for sample 1 at different environmental temperatures: 295 K, 195 K, and 10 K. As illustrated in the figure, the time for reaching the stability becomes shorter and shorter as T_0 decreases from 295 K to 10 K, indicating that the measured thermal diffusivity is increasing with decreasing temperature.

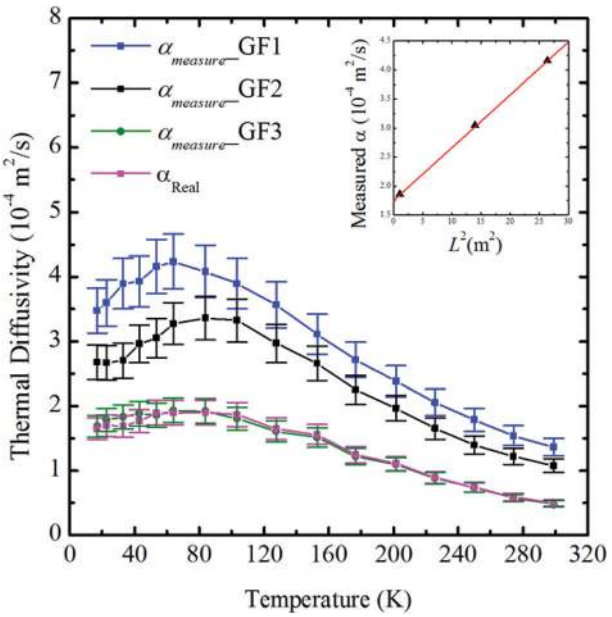

Fig. 3 The measured thermal diffusivity $\alpha_{measure}$ against temperature T for the three GF samples and the resulting real thermal diffusivity of GF (α_{real}). α_{real} follows a linear increase with decreasing temperature from 299 K to 104 K. At 104 K, α_{real} tends to be stable with a slight decrease from 43 K to 17 K. The top right inset is the measured thermal diffusivity against length square (L^2) for the three GF samples at a temperature of 54 K, showing one of the fitting process for determining the real thermal diffusivity of the sample. Triangles are for the experimental data, and the solid line represents the linear fitting.

3. Thermal properties and defect level

3.1. Thermal diffusivity of graphene foam and its variation against T

The result for $\alpha_{measure}$ of the three samples against real temperature T [=(T_0 + T_1)/2] is summarized in Fig. 3. Here, $\alpha_{measure}$ is still a combination of the real thermal diffusivity (α_{real}) and the radiation effect. The GF samples are cut from an equal-thickness GF film. From Table 1, the widths of the three samples are almost equal with an error of less than 0.8%. The lengths and widths were measured with INFINITY ANALYZE under the microscope with a high accuracy. From eqn (1), we can express $\alpha_{measure}$ as: $\alpha_{measure} = \alpha + 8\varepsilon_r\sigma T_0^3 L^2/\rho c_p D\pi^2$. Assuming uniform density, emissivity and α_{real} for the three samples, which is reasonable considering that they are actually the sample with different lengths, the radiation effect should be linearly related to its length square L^2. We plot the $\alpha_{measure}$–L^2 of the three samples at each temperature (see Fig. 3 inset for example). α_{real} is then obtained by linear fitting and extrapolating to the point of $L^2 = 0$. The real thermal diffusivity is also plotted in Fig. 3.

α_{real} shows an increasing behavior as T goes down from 299 K to 104 K. Below 104 K, α_{real} tends to be stable with a slight decrease from 43 K to 17 K. From the Wiedemann–Franz law, the contribution of electron transport to the thermal conductivity of graphene is negligible. The thermal behavior of graphene is governed by propagating phonons in the graphene lattice. The thermal transport ability of graphene is limited by phonon scattering in several mechanisms, mainly including Umklapp phonon–phonon scattering (U-scattering), phonon-defect scattering and phonon-boundary scattering. Only phonons with wave vectors (k_p) of the order of $G/2$ (G is the reciprocal lattice vector of the first Brillouin zone) participate in the U-scattering by collision. At near RT, the phonon energy is so high that almost all phonons possess high enough k_p to participate in the thermal transfer. Thus U-scattering dominates the scattering process at near RT. As T goes down, lattice elastic vibrations in graphene weaken and phonon population decreases. The U-scattering weakens correspondingly, which

results in increasing thermal diffusivity. At low temperatures (lower than 104 K), however, U-scattering becomes so weak that the defects and boundary scattering whose intensity is independent of the temperature begin to dominate. Thus, at the low temperature (from 104 K to 17 K), α_{real} tends to be stable, controlled by defects and boundary scattering. For the slight decrease at temperatures below 43 K, the reason has not been fully understood. It might be part of the intrinsic properties of the GF materials because we also found this 'dropping' thermal diffusivity in the data of pyrolytic graphite.[36] The surface area A_s contributing to the heat radiation could be much larger than $2(W + D)L$ due to the high porosity of the GF samples. Besides, for the three GF samples, larger 'dropping' of $\alpha_{measure}$ is observed for the longer samples than for the shorter one. Therefore, radiation could have a little effect on this "dropping" behavior.

3.2. Intrinsic thermal diffusivity and reffusivity of graphene

The intrinsic thermal diffusivity of graphene can be obtained using the thermal diffusivity of GF. Based on the model of Schuetz *et al.*,[37] a correlation has been demonstrated reliably for GF by H. Lin *et al.*[15] as $\alpha_G = 3\alpha_{GF}$. In this equation, α_G is the intrinsic thermal diffusivity of graphene, and α_{GF} is the thermal diffusivity of graphene foam. Using this equation, the thermal diffusivity of graphene can be calculated accurately without knowing the porosity of graphene foam. The uncertainty in measuring the volume fraction of graphene foam is therefore avoided.

The result for the intrinsic thermal diffusivity of graphene (α_G) is plotted in Fig. 4(a). The reciprocal of α_G is plotted in Fig. 4(b). Here α_G^{-1} is a new physical term called thermal reffusivity (denoted as Θ), which was firstly defined and used by Xu *et al.* to characterize the phonon thermal resistivity.[34] Just like electrical resistivity, thermal reffusivity is an intrinsic property of a material, which is solely determined by the phonon scattering inside materials. From the free electron model, electrical resistivity is expressed as the sum of phonon–phonon scattering and impurities scattering: $\rho = m/ne^2\tau = \rho_L + \rho_i$, where ρ_L is the resistivity caused by the thermal phonons and ρ_i is the resistivity sourced from the static defect scattering. For the same purpose, the thermal reffusivity is defined to characterize the phonon scattering for the thermal behavior. From the single relaxation time approximation, a classical model for phonon thermal conductivity can be expressed as: $\kappa = \rho c_p v^2\tau/3$. Here, v is the phonon velocity, which rarely changes with temperature. τ is the relaxation time for scattering. The reciprocal of κ cannot fully describe the phonon scattering since ρc_p also changes with temperature. Thus, the thermal reffusivity is defined as the reciprocal of thermal diffusivity to take out the specific heat effect. The above equation can thus be expressed in terms of thermal reffusivity as: $\Theta = \alpha^{-1} = 3/v^2\tau$. The relaxation time is inversely proportional to the phonon scattering intensity. Therefore, thermal reffusivity directly reflects the phonon scattering intensity. As will be discussed below, Θ also has two parts: one induced by phonon–phonon scattering and the other part by static phonon scattering by defects. Just like electrical resistivity, the variation of Θ *versus* temperature can be used to identify the residual value at the 0 K limit to evaluate the defect in the material. For metals, the heat capacity of electrons can be approximated as $C = \gamma T$, where C is the heat capacity per unit volume and γ is a constant. Therefore, for metals, the thermal conductivity becomes $\kappa = \gamma Tvl/3$. The thermal reffusivity for metals can be defined as $\Theta = T/\kappa$.

Thermal reffusivity can be used to characterize different scattering mechanisms. The way Θ changes with temperature and its residual value at the 0 K limit can all be used to provide unprecedented details of phonon scattering. Also, from the Θ–T curve, the Debye temperature can be determined. As mentioned above, the scattering mechanisms in graphene mainly include U-scattering, phonon-defect scattering and

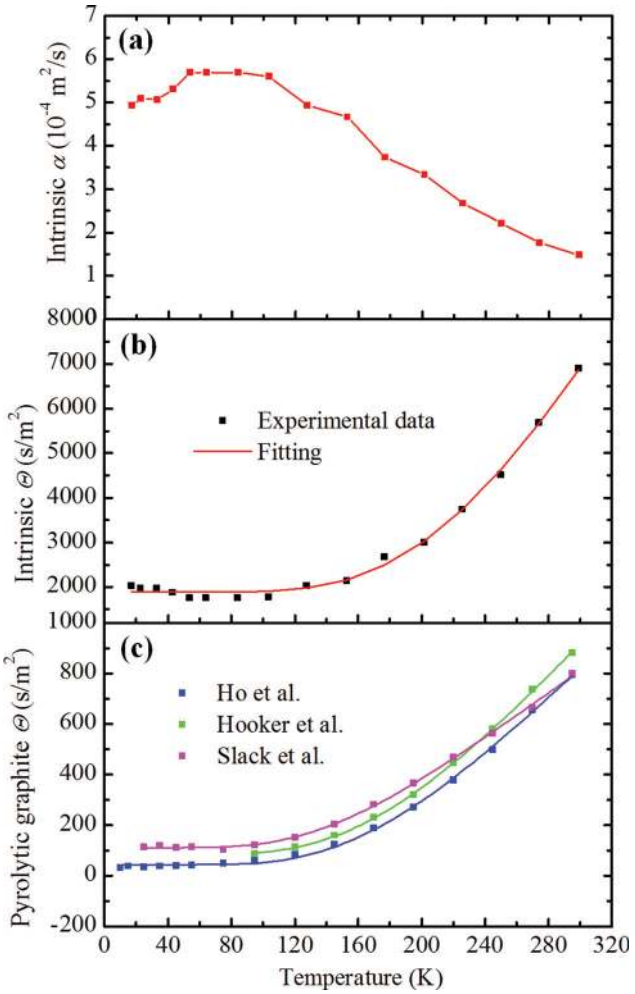

Fig. 4 (a) The intrinsic thermal diffusivity of graphene changes with temperature. (b) Thermal reffusivity of graphene compared with (c) the thermal reffusivity of other literature values for pyrolytic graphite.[36,40,41,48] The solid symbols are the experimental data, and the solid lines show the theoretical fitting of the data. As temperature approaches zero, the intersection point of the fitting line and the vertical axis is taken as the residual thermal reffusivity (Θ_0).

phonon-boundary scattering. According to Matthiessen's rule, it is generally a good approximation to linearly add all the scattering effects for the overall scattering effect:

$$\frac{1}{\tau_c} = \frac{1}{\tau_u} + \frac{1}{\tau_{defects}} + \frac{1}{\tau_{boundary}} \quad (2)$$

For U-scattering, lattice elastic vibration weakens as the temperature decreases, resulting in reduced U-scattering and increased relaxation time τ_u. Thus, as the temperature approaches 0 K, the overall reversed relaxation time ($1/\tau_c$) slowly reaches $1/\tau_{defects} + 1/\tau_{boundary}$. Thus Θ decreases to a constant: $\Theta(T \rightarrow 0) = 3/[v^2(\tau_{defect} + \tau_{boundary})]$, which correspondingly reflects the defect and boundary scattering effects in the thermal reffusivity. It is defined as the residual thermal reffusivity (Θ_0). For rare-defect crystallite materials, with no defects and boundary scattering existing, Θ is expected to be zero at the 0 K limit. To demonstrate this theory, we have studied some near-perfect materials in our previous work, for example, silicon, germanium, NaCl and NaF. When the temperature goes down to 0 K, their Θ truly decreases to zero just as the theory predicts.[34]

Fig. 4(b) shows the profile of the intrinsic thermal reffusivity of graphene varying with temperature. Clearly, Θ decreases as the temperature decreases from 299 K to 100 K. When T is below 100 K, Θ gradually becomes stable and comes to Θ_0. To compensate for the data fluctuation at low temperatures and reduce the error, the experimental data are fitted by a model of phonon-scattering. From solid state physics, the phonon population of U-scattering follows a behavior of $e^{-\theta/2T}$ at low temperatures,[38] where θ is the Debye temperature of graphene. Our experiments are conducted at temperatures much lower than θ (around 2000 K[39]). Combined with the residual thermal reffusivity theory, the model for thermal reffusivity is expressed as $\Theta = \Theta_0 + C \times e^{-\theta/2T}$, where C is a constant. Using OriginPro, the nonlinear curve fitting based on this equation for GF is $\Theta = 1878 + 1.03 \times 10^5 \times e^{-906.6\times T}$. Θ_0 is accordingly determined as 1878 s m^{-2} and θ is 1813 ± 48 K. For our graphene foam sample, the residual thermal reffusivity Θ_0 = 1878 s m^{-2}, taking about 27.2% of the RT reffusivity. The fitting is also plotted in Fig. 4(b) with the experimental data. The fitting line shows excellent agreement with the data, demonstrating the U-scattering effect on the thermal transport. Our resulting Debye temperature is 1813 K. Although many theoretical analyses suggested that the flexural acoustic (ZA) phonons provide the dominant contribution to the thermal transfer in graphene,[20] our value is very close to the average θ (=1911 K) of the three acoustic modes in graphene, which is 2840 K for longitudinal mode (LA), 1775 K for transverse mode (TA) and 1120 K for ZA.[20] This could result from the effect of the functional groups and other elements in GF as observed in XPS, which interrupt the phonon propagation and increase the energy coupling among ZA, LA and TA modes.

To further demonstrate our residual thermal reffusivity theory in graphene, we calculate the Θ evolution using some experimental data of pyrolytic graphite in the literature[36,40,41,48] and fit these data using our thermal reffusivity model $\Theta = \Theta_0 + C \times e^{-\theta/2T}$. The results are presented in Fig. 4(c) for comparison. As seen from Fig. 4(c), the model gives excellent fittings for the three data groups. All the three groups of Θ experience the same decreasing pattern as the temperature goes down. Finally they reach each Θ_0 value, which is determined by the different defect level in their samples. For the data from Ho *et al.*,[40] Hooker *et al.*[48] and Slack *et al.*,[36] the resulting residual thermal reffusivity Θ_0 are 43.3, 84.7 and 112.1 s m^{-2} respectively. Considering that their Θ at room temperature are 795.4 s m^{-2}, 881.8 s m^{-2} and 800.0 s m^{-2} respectively, the residual Θ_0 takes only about 5%, 9.6% and 14% of the whole reffusivity at room temperature. These results indicate the highly oriented graphene layers and low defect structure in those pyrolytic graphite samples. Their Debye temperatures are estimated as 1349 K, 1381 K and 1133 K respectively. Their estimated Debye temperatures are very close to the value of the ZA mode (1120 K), reflecting the dominance of the ZA mode phonon in heat conduction.

With the knowledge of Θ_0, the mean free path of phonons (l_s) induced by boundary and defect scattering can be estimated. l_s represents the average distance that a phonon travels between two scatterings. When the temperature approaches 0 K, U-scattering gradually vanishes, and the remaining scattering mechanisms are primarily boundary and defect scattering. When the temperature approaches absolute zero, the residual thermal reffusivity can be written as $\Theta_0 = 3/v^2(\tau_{defect} + \tau_{boundary}) = 3/vl_s$ under single relaxation time approximation. To calculate the phonon velocity, the phonon dispersion relation of graphite given by Wirtz *et al.*[42] is used. Phonon velocity is estimated as 9171 m s^{-1}, which is the average of the three branches: out-of-plane acoustic (ZA), longitudinal acoustic (LA), and transverse acoustic (TA). As a result, l_s from our data is estimated as 166 nm, which should be smaller than the crystallite sizes of GF. For some rare-defect materials, such as silicon and NaCl, the point defect scattering can be rather small. Their crystallite sizes can be estimated by l_s precisely using this method. For the pyrolytic graphite sample, the corresponding mean free paths from defect and boundary scattering are determined as 7.56 μm, 3.86 μm, and 2.92 μm for the data from Ho *et al.*, Hooker *et al.* and Slack *et al.*, respectively, which are close to the reported *a*-direction crystallite size of pyrolytic graphite.[43] These result further indicate the low defect level in the pyrolytic graphite samples.

3.3. Ideal thermal conductivity of graphene

By subtracting Θ_0 from Θ, the ideal thermal diffusivity is obtained by $\alpha_{ideal} = 1/(\Theta - \Theta_0)$. To reduce the error of data, we use the fitting data as Θ. Using α_{ideal} and the specific heat capacity of graphene, the ideal thermal conductivity of graphene can be determined as $\kappa_{ideal} = \rho c_p \alpha_{ideal}$, in which ρc_p is the volumetric specific heat of graphene. The literature thermal conductivity of graphene ranges from dozens to thousands of W m^{-1} K^{-1} due to the different defect levels in each

graphene sample. Using our method, the difficulties for measuring the defects levels in graphene samples can be averted. Instead, the defect effect can be identified by Θ_0. Fig. 5(a) shows the obtained ideal thermal diffusivity of graphene. α_{ideal} clearly has an $e^{\theta/2T}$ dependence, suggesting the dominating Umklapp phonon scattering mechanism.

By multiplying ρc_p, we are able to calculate κ_{ideal}. As far as we know, there has not been any experimental data for the specific heat of graphene at low temperatures. In the temperature range of 10 K to 300 K, the specific heat of graphite is normally taken as that of graphene. Fig. 5(b) presents the measured heat capacity of graphite by Desorbo *et al.*,[44] which is used here to calculate κ_{ideal}. Fig. 5(c) shows κ_{ideal} varying with temperature. At RT, κ_{ideal} is about 300 W m^{-1} K^{-1}. This value is much smaller than the previously reported thermal conductivity of 1500–5000 W m^{-1} K^{-1} for suspended graphene.[45] The difference might result from the curvatures and folds of graphene planes inside the GF sample as seen in SEM images [Fig. 1(b)], which largely increases the phonon scattering. In addition, there are other chemical elements (N, O, H and Si) and the residual functional group on the surface of the GF samples from the XPS results. For our GF, oxygen takes about 8.43% in the sample. It has been reported by Mu *et al.* that oxygen coverage of 5% reduced the graphene thermal conductivity by 90%.[46] These extra atoms inevitably distort the order of the lattice so as to interrupt the phonon propagation in graphene planes and even impede the neighboring planes. As the temperature goes down, κ_{ideal} increases all the way to 17 K, which further confirms the absence of the defect scattering effect. For the literature reported thermal conductivity profiles of graphene, their peaks occur at temperatures from 100 K to near RT. The peak position was determined by the defect level in graphene samples. It has been suggested that as the perfection of the graphite samples is improved, the peak of thermal conductivity shifts from RT to about 80 K.[47] In our result, since the defect effect has been completely subtracted, α_{ideal} increases all the way as expected. Numerous studies suggest that the specific heat of graphite follows the Debye T^3 law at very low temperature (<10 K), and transforms to $\sim T^2$ in the intermediate temperature range (10–100 K). The thermal diffusivity of graphene has a temperature dependence as $\alpha_{ideal} \sim e^{\theta/2T}$. Therefore, the resulting thermal conductivity should have a behavior of $\kappa_{ideal} \sim T^2 \times e^{\theta/2T}$, where θ = 1813 K in our work. As the temperature goes down from 300 K to 10 K, $e^{1813/2T}$ increases faster than the decreasing rate of T^2. Accordingly, κ_{ideal} increases with decreasing temperature all the way. The ideal thermal conductivity of pyrolytic graphite was also calculated from the literature data using our model. It can be seen from Fig. 5(c) that κ_{ideal} of the three pyrolytic graphite follow the same pattern as the temperature goes down.

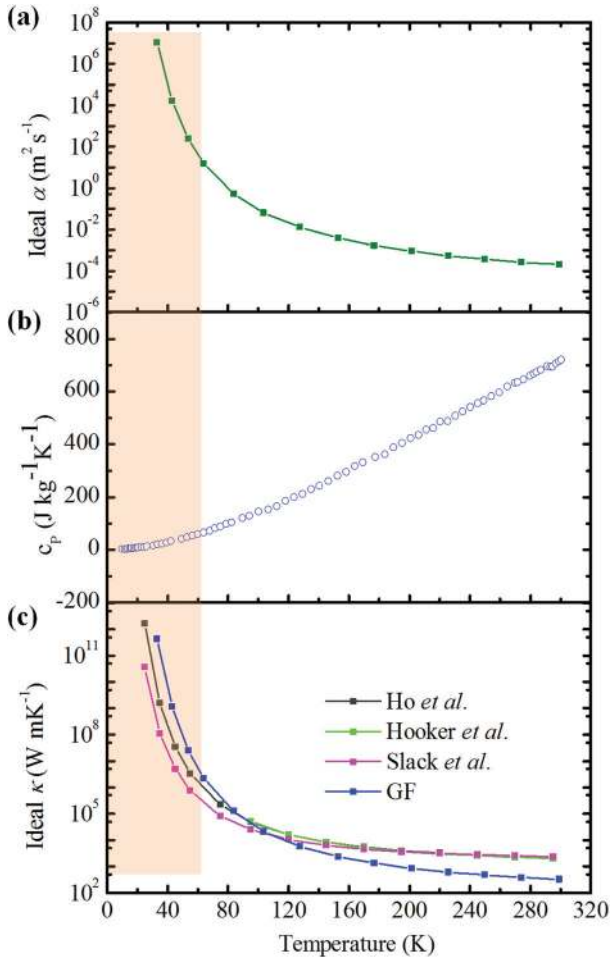

Fig. 5 (a) The ideal thermal diffusivity of graphene. (b) The experimental data for specific heat of graphite.[44] (c) The ideal thermal conductivity of graphene (κ_{ideal}) against temperature compared with what we obtained from other literature data of pyrolytic graphite.[36,40,41,48] The data inside the orange rectangle (below 80 K) are less reliable due to the error of α_G at low temperatures and the undecided difference of specific heat between graphene and graphite.

Our κ_{ideal} value is smaller than that of pyrolytic graphite at near RT (100–299 K), while it exceeds the value of pyrolytic graphite below 100 K. This demonstrates the superior thermal conductivity of graphene compared with pyrolytic graphite. As the temperature goes down, κ_{ideal} increases rapidly and goes beyond 10^5 W m^{-1} K^{-1} below 80 K based on our calculations. The data below 80 K should be used with less confidence since the specific heat values are taken from graphite experiments, which may be higher than the real specific heat of graphene.[14] In addition, the error of fitted thermal reffusivity is larger at low temperatures due to the data perturbation at low temperatures, which results in the larger error in the value of ideal thermal diffusivity. In this work, the low temperature range is chosen in order to identify the defect level of graphene foam. These results illustrate the phonon scattering mechanism in graphene at low temperatures and shed light on understanding the thermal behavior of graphene-based materials against temperature variation. The ideal thermal conductivity of graphene and the corresponding scattering mechanisms at high temperatures (room temperature to 1000 °C) will be further investigated in the near future once our new high-temperature vacuum stage is ready to use.

4. Conclusion

This work investigated the thermal transport in graphene foam from RT to 17 K using the TET technique. The three-dimensional interconnected foam-like samples basically consist of four-layered graphene. The XPS result uncovers the chemical composition of carbon (89%), oxygen (8.43%), nitrogen (0.43%), and silicon (2.14%). The N 1s spectrum indicates the presence of a small amount of NH–C═O functional group on the surface of the GF sample. The intrinsic thermal diffusivity (α_G) of graphene is accurately determined after subtracting the radiation effect. We identified the defect-induced phonon scattering effects in thermal transport of graphene by fitting the thermal reffusivity Θ to the point of $T = 0$ K. Using the residual thermal reffusivity (Θ_0), we are able to evaluate the Debye temperature and the defect-phonon scattering mean free path of graphene. Θ_0 is found to be 1878 s m^{-2} for the studied graphene foam, and 43–112 s m^{-2} for three highly crystalline graphite materials. This indicates the orders of magnitude higher defect level in the GF. The defect-induced phonon scattering gave a long mean free path of 166 nm. The Debye temperature of graphene was determined at 1813 K, agreeing well with the average theoretical Debye temperature (1911 K) of TA, ZA, and LA phonons in graphene. By subtracting the residual thermal reffusivity, we obtained the ideal thermal diffusivity and conductivity of the studied graphene. The ideal thermal conductivity (κ_{ideal}) resulting from Umklapp phonon–phonon scattering was found to increase all the way up with decreasing temperature. At RT, κ_{ideal} is around 300 W m^{-1} K^{-1}. It could go up to greater than 10^5 W m^{-1} K^{-1} when the temperature goes down to 80 K. The ideal thermal conductivity of several reference graphite samples shows a similar trend and comparable results.

Acknowledgements

Army Research Office (W911NF-12-1-0272), Office of Naval Research (N000141210603), and National Science Foundation (CBET1235852, CMMI1264399, and CMMI1200397) are gratefully acknowledged for support of this work. X.W. acknowledges the partial support from the "Eastern Scholar" Program of Shanghai, China. Y.X is supported by the China Scholarship Council.

Notes and references

1 M. A. Worsley, P. J. Pauzauskie, T. Y. Olson, J. Biener, J. H. Satcher and T. F. Baumann, *J. Am. Chem. Soc.*, 2010, **132**, 14067–14069.
2 A. A. Balandin, S. Ghosh, W. Z. Bao, I. Calizo, D. Teweldebrhan, F. Miao and C. N. Lau, *Nano Lett.*, 2008, **8**, 902–907.
3 H. Y. Sun, Z. Xu and C. Gao, *Adv. Mater.*, 2013, **25**, 2554–2560.
4 C. Wang, L. Zhang, Z. H. Guo, J. G. Xu, H. Y. Wang, K. F. Zhai and X. Zhuo, *Microchim. Acta*, 2010, **169**, 1–6.
5 F. Bonaccorso, Z. Sun, T. Hasan and A. C. Ferrari, *Nat. Photonics*, 2010, **4**, 611–622.
6 S. Ghosh, I. Calizo, D. Teweldebrhan, E. P. Pokatilov, D. L. Nika, A. A. Balandin, W. Bao, F. Miao and C. N. Lau, *Appl. Phys. Lett.*, 2008, **92**, 151911–151911.
7 X. Wang, L. J. Zhi and K. Mullen, *Nano Lett.*, 2008, **8**, 323–327.
8 H. L. Wang, L. F. Cui, Y. A. Yang, H. S. Casalongue, J. T. Robinson, Y. Y. Liang, Y. Cui and H. J. Dai, *J. Am. Chem. Soc.*, 2010, **132**, 13978–13980.
9 D. Cohen-Tanugi and J. C. Grossman, *Nano Lett.*, 2012, **12**, 3602–3608.
10 X. M. Sun, Z. Liu, K. Welsher, J. T. Robinson, A. Goodwin, S. Zaric and H. J. Dai, *Nano Res.*, 2008, **1**, 203–212.
11 S. S. Chen, Q. Z. Wu, C. Mishra, J. Y. Kang, H. J. Zhang, K. J. Cho, W. W. Cai, A. A. Balandin and R. S. Ruoff, *Nat. Mater.*, 2012, **11**, 203–207.
12 J. U. Lee, D. Yoon, H. Kim, S. W. Lee and H. Cheong, *Phys. Rev. B: Condens. Matter*, 2011, **83**, 081419.
13 C. Faugeras, B. Faugeras, M. Orlita, M. Potemski, R. R. Nair and A. K. Geim, *ACS Nano*, 2010, **4**, 1889–1892.
14 E. Pop, V. Varshney and A. K. Roy, *MRS Bull.*, 2012, **37**, 1273–1281.
15 H. Lin, S. Xu, X. W. Wang and N. Mei, *Nanotechnology*, 2013, **24**, 415706.
16 W. W. Cai, A. L. Moore, Y. W. Zhu, X. S. Li, S. S. Chen, L. Shi and R. S. Ruoff, *Nano Lett.*, 2010, **10**, 1645–1651.
17 J. H. Chen, C. Jang, S. Adam, M. S. Fuhrer, E. D. Williams and M. Ishigami, *Nat. Phys.*, 2008, **4**, 377–381.
18 H. C. Schniepp, J. L. Li, M. J. McAllister, H. Sai, M. Herrera-Alonso, D. H. Adamson, R. K. Prud'homme, R. Car, D. A. Saville and I. A. Aksay, *J. Phys. Chem. B*, 2006, **110**, 8535–8539.
19 D. L. Nika, E. P. Pokatilov, A. S. Askerov and A. A. Balandin, *Phys. Rev. B: Condens. Matter*, 2009, **79**, 155413.
20 J. C. Zhang, X. P. Huang, Y. N. Yue, J. M. Wang and X. W. Wang, *Phys. Rev. B: Condens. Matter*, 2011, **84**, 235416.
21 W. J. Evans, L. Hu and P. Keblinski, *Appl. Phys. Lett.*, 2010, **96**, 203112.
22 L. Lindsay, D. A. Broido and N. Mingo, *Phys. Rev. B: Condens. Matter*, 2010, **82**, 161402.
23 E. Munoz, J. X. Lu and B. I. Yakobson, *Nano Lett.*, 2010, **10**, 1652–1656.
24 F. Yavari, Z. P. Chen, A. V. Thomas, W. C. Ren, H. M. Cheng and N. Koratkar, *Sci. Rep.*, 2011, **1**, 166.
25 Y. Zhao, J. Liu, Y. Hu, H. H. Cheng, C. G. Hu, C. C. Jiang, L. Jiang, A. Y. Cao and L. T. Qu, *Adv. Mater.*, 2013, **25**, 591–595.
26 N. Li, Q. Zhang, S. Gao, Q. Song, R. Huang, L. Wang, L. W. Liu, J. W. Dai, M. L. Tang and G. S. Cheng, *Sci. Rep.*, 2013, **3**, 1604.

27 M. T. Pettes, H. X. Ji, R. S. Ruoff and L. Shi, *Nano Lett.*, 2012, **12**, 2959–2964.
28 D. Graf, F. Molitor, K. Ensslin, C. Stampfer, A. Jungen, C. Hierold and L. Wirtz, *Nano Lett.*, 2007, **7**, 238–242.
29 E. V. Castro, K. S. Novoselov, S. V. Morozov, N. M. R. Peres, J. M. B. L. Dos Santos, J. Nilsson, F. Guinea, A. K. Geim and A. H. Castro Neto, *Phys. Rev. Lett.*, 2007, **99**, 216802.
30 Z. Q. Luo, S. H. Lim, Z. Q. Tian, J. Z. Shang, L. F. Lai, B. MacDonald, C. Fu, Z. X. Shen, T. Yu and J. Y. Lin, *J. Mater. Chem.*, 2011, **21**, 8038–8044.
31 X. H. Feng and X. W. Wang, *Thin Solid Films*, 2011, **519**, 5700–5705.
32 X. Feng, X. Wang, X. Chen and Y. Yue, *Acta Mater.*, 2011, **59**, 1934–1944.
33 J. Q. Guo, X. W. Wang and T. Wang, *J. Appl. Phys.*, 2007, **101**, 063537.
34 Z. L. Xu, X. W. Wang and H. Q. Xie, *Polymer*, 2014, **55**, 6373–6380.
35 G. Q. Liu, X. P. Huang, Y. J. Wang, Y. Q. Zhang and X. W. Wang, *Soft Matter*, 2012, **8**, 9792–9799.
36 G. A. Slack, *Phys. Rev.*, 1962, **127**, 694–701.
37 M. A. Schuetz and L. R. Glicksman, *J. Cell Plast.*, 1984, **20**, 114–121.
38 C. Kittel and P. McEuen, *Introduction to solid state physics*, J. Wiley, Hoboken, NJ, 8th edn, 2005, p. 126.
39 L. A. Falkovsky, *Phys. Rev. B: Condens. Matter*, 2007, **75**, 033409.
40 C. Y. Ho, R. W. Powell and P. E. Liley, *Thermal conductivity of the elements: a comprehensive review*, American Chemical Society, Washington, 1975, p. 150.
41 S. S. Chen, A. L. Moore, W. W. Cai, J. W. Suk, J. H. An, C. Mishra, C. Amos, C. W. Magnuson, J. Y. Kang, L. Shi and R. S. Ruoff, *ACS Nano*, 2011, **5**, 321–328.
42 L. Wirtz and A. Rubio, *Solid State Commun.*, 2004, **131**, 141–152.
43 R. A. Morant, *J. Phys. D: Appl. Phys.*, 1970, **3**, 1367–1373.
44 W. Desorbo and W. W. Tyler, *J. Chem. Phys.*, 1953, **21**, 1660–1663.
45 A. A. Balandin, *Nat. Mater.*, 2011, **10**, 569–581.
46 X. Mu, X. F. Wu, T. Zhang, D. B. Go and T. F. Luo, *Sci. Rep.*, 2014, **4**, 3909.
47 J. W. Klett, A. D. McMillan, N. C. Gallego and C. A. Walls, *J. Mater. Sci.*, 2004, **39**, 3659–3676.
48 C. N. Hooker, A. R. Ubbelohd and D. A. Young, *Proc. R. Soc. London, Ser. A*, 1965, **284**, 17.